Research Article | Vol. 24, No. 19 | 19 Sep 2016 | OPTICS EXPRESS 21897

Optics EXPRESS

Development of regenerated fiber Bragg grating sensors with long-term stability

MERT CELIKIN,[1] DAVID BARBA,[1] BINOD BASTOLA,[1] ANDREAS RUEDIGER,[1,3] AND FEDERICO ROSEI[1,2,4]

[1]*Centre Énergie Matériaux Télécommunications, Institut National de la Recherche Scientifique, Varennes, Quebec, J3X 1S2, Canada*
[2]*Institute for Fundamental and Frontier Science, University of Electronic Science and Technology of China,Chengdu, China*
[3]*ruediger@emt.inrs.ca*
[4]*rosei@emt.inrs.ca*

Abstract: The effect of annealing cycle on regeneration efficiency was investigated through isothermal treatments between 700 and 1000°C. We determined an inverse relationship between the recovery rate of the peak reflectivity and temperature. A regeneration efficiency of 85.2% and long-term stability at 1000°C for 500 hours were achieved via a slow regeneration process. Thermal sensors developed by isothermal regeneration were determined to be reliable up to 1000°C (±2 °C). Experimental findings suggest the involvement of both diffusion related phenomena and stress variation through densification of the fiber core in type-I FBG during the thermal regeneration process.

OCIS codes: (060.3735) Fiber Bragg gratings; (060.2370) Fiber optics sensors; (060.2300) Fiber measurements; (230.1480) Bragg reflectors; (250.5230) Photoluminescence.

References and Links

1. S. J. Mihailov, "Fiber Bragg grating sensors for harsh environments," Sensors (Basel) **12**(2), 1898–1918 (2012).
2. L. Polz, Q. Nguyen, H. Bartelt, and J. Roths, "Fiber Bragg gratings in hydrogen-loaded photosensitive fiber with two regeneration regimes," Opt. Commun. **313**, 128–133 (2014).
3. D. Barrera and S. Sales, "A high-temperature fiber sensor using a low cost interrogation scheme," Sensors **13**(9), 11653–11659 (2013).
4. A. Bueno, D. Kinet, P. Mégret, and C. Caucheteur, "Fast thermal regeneration of fiber Bragg gratings," Opt. Lett. **38**(20), 4178–4181 (2013).
5. D. Barrera, V. Finazzi, J. Villatoro, S. Sales, and V. Pruneri, "Packaged optical sensors based on regenerated fiber bragg gratings for high temperature applications," IEEE Sens. J. **12**(1), 107–112 (2012).
6. S. Bandyopadhyay, J. Canning, P. Biswas, M. Stevenson, and K. Dasgupta, "A study of regenerated gratings produced in germanosilicate fibers by high temperature annealing," Opt. Express **19**(2), 1198–1206 (2011).
7. E. Lindner, C. Chojetztki, S. Brueckner, M. Becker, M. Rothhardt, J. Vlekken, and H. Bartelt, "Arrays of regenerated fiber bragg gratings in non-hydrogen-loaded photosensitive fibers for high-temperature sensor networks," Sensors **9**(10), 8377–8381 (2009).
8. A. Gillooly, "Photosensitive fibres: growing gratings," Nat. Photonics **5**(8), 468–469 (2011).
9. M. Celikin, D. Barba, A. Ruediger, M. Chicoine, F. Schiettekatte, and F. Rosei, "Co-mediated nucleation of erbium/silicon nanoclusters in fused silica," J. Mater. Res. **30**(20), 3003–3010 (2015).
10. D. S. Bykov, O. A. Schmidt, T. G. Euser, and P. S. J. Russell, "Flying particle sensors in hollow-core photonic crystal fibre," Nat. Photonics **9**(7), 461–465 (2015).
11. E. Udd and W. B. Spillman, *Fiber Optic Sensors: An Introduction for Engineers and Scientists*, 2nd ed. (2011).
12. F. K. Coradin, V. De Oliveira, M. Muller, H. J. Kalinowski, and J. L. Fabris, "Long-term stability decay of standard and regenerated Bragg gratings tailored for high temperature operation," J. Microw. Optoelectron. Electromagn. Appl. **12**(2), 719–729 (2013).
13. P. Holmberg, F. Laurell, and M. Fokine, "Influence of pre-annealing on the thermal regeneration of fiber Bragg gratings in standard optical fibers," Opt. Express **23**(21), 27520–27535 (2015).
14. J. Canning, S. Bandyopadhyay, M. Stevenson, P. Biswas, J. Fenton, and M. Aslund, "Regenerated gratings," J. Eur. Opt. Soc. **4**, 09052 (2009).
15. K. Cook, L. Y. Shao, and J. Canning, "Regeneration and helium: Regenerating Bragg gratings in helium-loaded germanosilicate optical fibre," Opt. Mater. Express **2**(12), 1733–1742 (2012).
16. T. Wang, L. Y. Shao, J. Canning, and K. Cook, "Regeneration of fiber Bragg gratings under strain," Appl. Opt. **52**(10), 2080–2085 (2013).

#272635 http://dx.doi.org/10.1364/OE.24.021897
Journal © 2016 Received 2 Aug 2016; revised 7 Sep 2016; accepted 8 Sep 2016; published 12 Sep 2016

Optics EXPRESS

17. Y. K. Cheong, W. Y. Chong, S. S. Chong, K. S. Lim, and H. Ahmad, "Regenerated type-IIa fibre Bragg grating from a Ge-B codoped fibre via thermal activation," Opt. Laser Technol. **62**, 69–72 (2014).
18. J. Canning, M. Stevenson, S. Bandyopadhyay, and K. Cook, "Extreme silica optical fibre gratings," Sens. **8**(10), 6448–6452 (2008).
19. S. Bandyopadhyay, J. Canning, M. Stevenson, and K. Cook, "Ultrahigh-temperature regenerated gratings in boron-codoped germanosilicate optical fiber using 193 nm," Opt. Lett. **33**(16), 1917–1919 (2008).
20. R. Kashyap, *Fiber Bragg Gratings* (Academic, 1999).
21. J. J. Zhu, A. P. Zhang, B. Zhou, F. Tu, J. T. Guo, W. J. Tong, S. He, and W. Xue, "Effects of doping concentrations on the regeneration of Bragg gratings in hydrogen loaded optical fibers," Opt. Commun. **284**(12), 2808–2811 (2011).
22. K. E. Chisholm, K. Sugden, and I. Bennion, "Effects of thermal annealing on Bragg fibre gratings in boron/germania co-doped fibre," J. Phys. D Appl. Phys. **31**(1), 61–64 (1998).
23. S. Pal, J. Mandal, T. Sun, and K. T. V. Grattan, "Analysis of thermal decay and prediction of operational lifetime for a type I boron-germanium codoped fiber Bragg grating," Appl. Opt. **42**(12), 2188–2197 (2003).
24. M. H. Lai, K. S. Lim, D. S. Gunawardena, H. Z. Yang, W. Y. Chong, and H. Ahmad, "Thermal stress modification in regenerated fiber Bragg grating via manipulation of glass transition temperature based on CO_2-laser annealing," Opt. Lett. **40**(5), 748–751 (2015).
25. K. S. Lim, H. Z. Yang, W. Y. Chong, Y. K. Cheong, C. H. Lim, N. M. Ali, and H. Ahmad, "Axial contraction in etched optical fiber due to internal stress reduction," Opt. Express **21**(3), 2551–2562 (2013).
26. T. Erdogan, V. Mizrahi, P. J. Lemaire, and D. Monroe, "Decay of ultraviolet-induced fiber Bragg gratings," J. Appl. Phys. **76**(1), 73–80 (1994).
27. S. Pal, "Characterization of thermal (in)stability and temperature-dependence of type-I and type-IIA Bragg gratings written in B-Ge co-doped fiber," Opt. Commun. **262**(1), 68–76 (2006).
28. G. Brambilla and H. Rutt, "Fiber Bragg gratings with enhanced thermal stability," Appl. Phys. Lett. **80**(18), 3259–3261 (2002).
29. V. Grubsky, D. Starodubov, and W. W. Morey, "High-temperature Bragg gratings in germanosilicate fibers," in *Bragg Gratings, Photosensitivity, and Poling in Glass Waveguides*, Technical Digest (Optical Society of America, 2003), paper MB5.
30. S. Pal, T. Sun, K. T. V. Grattan, S. A. Wade, S. F. Collins, G. W. Baxter, B. Dussardier, and G. Monnom, "Bragg gratings written in Sn-Er-Ge-codoped silica fiber: investigation of photosensitivity, thermal stability, and sensing potential," J. Opt. Soc. Am. A **21**(8), 1503–1511 (2004).
31. Y. Zhou and Z. Gu, "The study of removing hydroxyl from silica glass," J. Non-Cryst. Solids **352**(38-39), 4030–4033 (2006).
32. D. Barba, F. Martin, K. Tagziria, M. Nicklaus, É. Haddad, F. Rosei, and A. Ruediger, "Photoluminescence mapping of oxygen-defect emission for nanoscale spatial characterization of fiber Bragg gratings," J. Appl. Phys. **116**(6), 064906 (2014).
33. L. Skuja, "Defect studies in vitreous silica and related materials: Optically active oxygen-deficiency-related centers in amorphous silicon dioxide," J. Non-Cryst. Solids **239**(1-3), 16–48 (1998).
34. L. Skuja, "The origin of the intrinsic 1.9 eV luminescence band in glassy SiO_2," J. Non-Cryst. Solids **179**, 51–69 (1994).
35. L. Skuja, T. Suzuki, and K. Tanimura, "Site-selective laser-spectroscopy studies of the intrinsic 1.9-eV luminescence center in glassy SiO2," Phys. Rev. B Condens. Matter **52**(21), 15208–15216 (1995).
36. M. Fokine, "Thermal stability of chemical composition gratings in fluorine-germanium-doped silica fibers," Opt. Lett. **27**(12), 1016–1018 (2002).
37. M. Fokine, "Growth dynamics of chemical composition gratings in fluorine-doped silica optical fibers," Opt. Lett. **27**(22), 1974–1976 (2002).

1. Introduction

Optical fiber based devices such as Fiber Bragg Grating (FBG) sensors have become highly attractive for nuclear, submarine, aerospace and space applications due to their resistance to electromagnetic interference, low density, mechanical flexibility, as well as great configurability [1–10]. A standard (type-I) FBG consists of a protective silica fiber cladding surrounding a photosensitive germanosilicate glass fiber core where periodic gratings are obtained by UV-inscription through a micrometric mask [11]. The periodic modulation of the refractive index generates highly selective spectral filtering effects that can be used to measure temperature and pressure in real time [8]. However, the sensing capability of FBGs, which depends on peak reflectivity with precise wavelength, degrades with temperature, limiting their implementation in power generating stations, space exploration modules and engine turbines [6].

In the last decade, different types of FBGs with superior thermal stability (Type-II, Type-In, Chemical Composition Gratings (CCG) and Regenerated Fiber Bragg Gratings (RFBG))

Optics EXPRESS

were developed in attempts to increase the thermal resistance of standard type-I gratings that can function only up to 425°C [4, 12, 13]. While CCG and RFBG have both shown superior performances, withstanding temperatures above 1000°C with exploitable spectral quality for operation in harsh environments over a few hours [4, 13, 14] to date there is still a strong controversy about the underlying mechanism of the so-called 'thermal regeneration' [12]. The challenge in understanding the regeneration phenomenon relates to the complex processing steps involving numerous parameters which affect the regeneration efficiency, defined as the percentage of the seed-grating reflectivity that remains upon regeneration [2, 4, 12, 15]. Gas loading (H_2 or Helium), pre-annealing, UV-inscription power and laser wavelength, the strength of initial (seed) grating and annealing cycle, as well as material properties such as fiber composition were all found to influence thermal recovery [2, 4, 12, 15]. In addition, strain is another important factor which affects the central wavelength and the thermal regeneration efficiency [1, 16]. The reported recovery rates vary enormously from 4% up to 74% depending on the parameters mentioned earlier [4, 6, 7, 17]. Maximizing the recovery rate upon regeneration is crucial for the development of FBG sensors with long-term stability, as peak reflectivity will be available for temperature measurements for longer durations.

This work focuses on the effect of annealing temperature on the regeneration process. In previous studies, two annealing approaches were mainly used for the thermal regeneration of FBGs; i) the first approach involves a single step continuous rise in temperature using a constant heating rate from room temperature (RT) up to 1000°C and above, whereas ii) in the second approach, the FBG is heated from RT to an intermediate temperature (~850–900°C), held isothermally for 10 to 60 minutes and then ramped up to 1000°C and above [4, 6,16, 18, 19]. The ultimate regeneration efficiency was reported to be superior when thermal regeneration occurs during isothermal holding at an intermediate temperature below 1000°C, in comparison with an annealing cycle where regeneration takes place during continuous heating up to 1000°C and above [6]. However, the value of this intermediate temperature used for isothermal treatments is dependent on seed grating strength, composition, dopant concentration and hydrogen loading [4]. Hence, this intermediate temperature, which is specific to the FBG under study, needs to be determined empirically before each thermal regeneration experiment. For FBGs with same processing route, even using different holding temperatures and annealing cycles allowed thermal regeneration and caused significant variations in recovery rates [4, 6].

Here we primarily investigate the effect of isothermal annealing in the 700-1000°C temperature range for thermal regeneration and also study the process dynamics to maximize recovery efficiency and long-term stability. Our experimental approach is based on the simultaneous measurements of FBG peak reflectivity, its Bragg wavelength and peak width, whose time evolutions were reported for FBGs of same origin, composition and optical properties. RFBG developed in this work were also tested for their reliability to be used as thermal sensors via calibration experiments up to 1000°C. Photoluminescence (PL) measurements were conducted on FBGs before and after regeneration for supplementary information. We finally compared our experimental findings with existing theories on the origin of the thermal regeneration mechanism.

2. Theoretical background

The reflection by a uniform FBG can be described by using four parameters: a central wavelength λ_B, the peak reflectivity, denoted as ρ_B, the peak width ω_B and the surrounding noise level which is primarily determined by the sensitivity of the detector. The Bragg wavelength obeys the following relation [13, 20]:

$$\lambda_B = 2n_{eff}\Lambda \quad (1)$$

Optics EXPRESS

where n_{eff} is the effective modal index of the fiber around 1.5 μm ($n_{cladding} < n_{eff} < n_{core}$) and Λ is the period of the refractive index modulation inside the fiber core. The peak reflectivity (ρ_B) of spectral width (ω_B) for strong gratings ($\Delta n_m > \sim 1.10^{-4}$) is given by the relation [13, 20]:

$$\rho_B = \tan h^2\left(\frac{\pi\eta\Delta n_m N}{2n_{eff}}\right) \tag{2}$$

$$\omega_B \propto \Delta n_m \lambda_B \tag{3}$$

where η is the overlap integral of the guided mode in the fiber core, N is the number of periodic variation (~$2\cdot10^4$ in our case) and Δn_m is the average amplitude of the refractive index modulation.

3. Experimental

The UV-inscription of commercial photosensitive optical silica fibers (IXFiber; 8.2 μm core diameter, 125 μm outside cladding diameter) containing 3.5 mole % GeO_2 to produce type-I FBGs was conducted at MPB Technologies Inc. Laboratories. Prior to FBG writing, the fibers were loaded with deuterium (D) under high pressures (~2000 psi) at room temperature (RT) for 120 hours. After conducting a low temperature heat treatment (120 °C, 1 day), type-I (seed) FBGs with a transmission loss of - 33 (+/– 2) dB and grating length of 10 mm were obtained via pulsed UV inscription (λ: 193 nm, power: 4-5 mJ, frequency: 70 Hz).

An erbium broadband laser source (1530-1565 nm) was used throughout the annealing cycles and reflectivity measurements were recorded *in situ* with 10 seconds (1 to 10 minutes at T = 700 °C) acquisition time via a Burleigh WA-7000 Multi-Line wavemeter of 0.5 pm wavelength measurement resolution. Additionally, reflectivity and transmission measurements of all fibers before and after regeneration were conducted using an Optical Spectrum Analyzer (OSA). Peak reflection values are presented as relative optical power in dB scale. The recovery rate of the peak reflectivity is based on the transmitted signal [6]. The experimental setup for high temperature regeneration experiments is depicted in Fig. 1.

Type-I gratings were annealed in steps with a constant heating rate of 25 °C/min between each step. For short-term stabilization and to compensate overshooting, samples are held for 5 minutes at each step. Firstly, the temperature was ramped up from RT to 500 °C and then using 100 °C temperature increments (50 - 200 °C for the final temperature raise depending on T_{final}), we reached T_{final} between 700°C and 1000°C. For T_{final} values above 900 °C, a direct ramp from 800 °C was used to avoid the onset of regeneration prior to reaching T_{final}, thereby ensuring for all samples that regeneration occurred at (stabilized) T_{final}. T_{final} is kept constant (± 1°C) until the regeneration process is complete and the variation in reflectivity is negligible (< 0.2 dB). Finally, the samples are cooled down to RT inside the furnace before OSA transmission measurements. The data were extracted with a dedicated Matlab code.

For calibration of λ_B shifts and the quality assessment of thermally regenerated FBG sensors, temperature measurements from 26 °C to 1000 °C with four repetitions were done. The calibration curves were drawn for RFBG sensors upon long-term annealing cycles.

Confocal PL measurements were performed, before and after regeneration, using an Olympus BX71 microscope, coupled to a Horiba iHR320 spectrometer equipped with a thermoelectrically cooled CCD array and a 0.9 N.A objective mounted orthogonally for both excitation and collection of the emission. The FBG is excited perpendicular to the fiber axis using the TEM00 mode of a 473 nm solid state laser, corresponding to a sample volume associated within a prolate ellipsoid of about 3 microns in height, with a radius of the airy disc of ~350 nm. The fiber is fixed horizontally on the X-Y-Z scanner, whose vertical position (Z) is adjusted from interfacial reflections to position the optical focus inside the fiber core, with a precision of about +/– 1 μm.

Optics EXPRESS

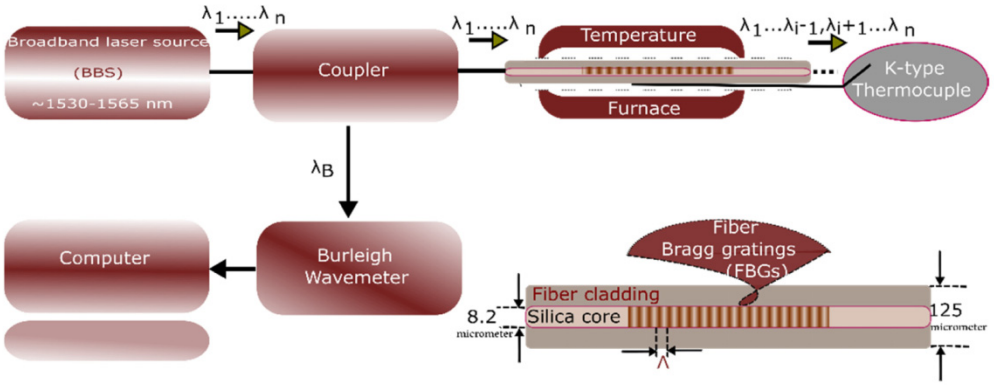

Fig. 1. Experimental setup for high temperature *in situ* reflectivity measurements.

4. Thermal regeneration experiments

Thermal regeneration experiments were conducted at different final temperatures (T_{final}) on FBGs with initial seed grating strength of about −33 dB, fabricated using similar processes. A representation of the complete heating cycle is shown by the wavelength vs. time graph for a T_{final} of 900 °C [Fig. 2]. Except for the experiment at 1000 °C, where T_{final} is reached just before the disappearance of the Bragg peak, ramping to the final temperatures are completed in all samples before a major decrease in peak reflectivity and regeneration occurs. We found that regeneration takes place at all T_{final} used (700-1000 °C), with different kinetics. The variation of peak reflectivity as well as peak width with time is given in Fig. 3 for T_{final} values ranging from 900 to 1000 °C. We define the recovery time during which the peak reflectivity is not measurable as τ_{rec} [Fig. 3]. As vertical arrows indicate the time (t_0) when ramping to T_{final} is completed, the onset time of peak width decrease occurs at a much earlier stage than the decrease in peak reflectivity. Even though the change of total refractive index already occurs around 300 °C, the effect on the peak reflectivity only becomes detectable later, often after T_{final} was reached. This feature stems from the relationships given by Eqs. (2) and (3), where the peak width varies linearly with the refractive index [Eq. (3)] as compared to a highly non-linear relation for the reflectivity [Eq. (2)]. The FBG remains an almost perfect mirror at λ_B even though the refractive index modulation decreases. In other words, structural or stress variations occur, resulting in a change in refractive index modulation at an early stage (≈300°C, after 6-7 minutes of heating) in the regeneration process, yet the effect of this change can only be observed by peak reflectivity variation at a later stage. We operate FBGs with roughly 20,000 periods so even though the penetration depth of the beam at λ_B increases with decreasing refractive index modulation, the combination of this modulation with the length guarantees almost 100% reflectivity until the modulation becomes too low to be compensated by the length of the grating.

Upon heating from ambient temperature to the maximum temperature [Fig. 2], λ_B shifts almost linearly with a temperature coefficient of approximately 13 pm/K towards longer wavelengths following Eq. (1) in which, both the FBG periodicity (thermal expansion) and the mean refractive index (thermo-optic effect) of the fiber core depend on temperature.

Optics EXPRESS

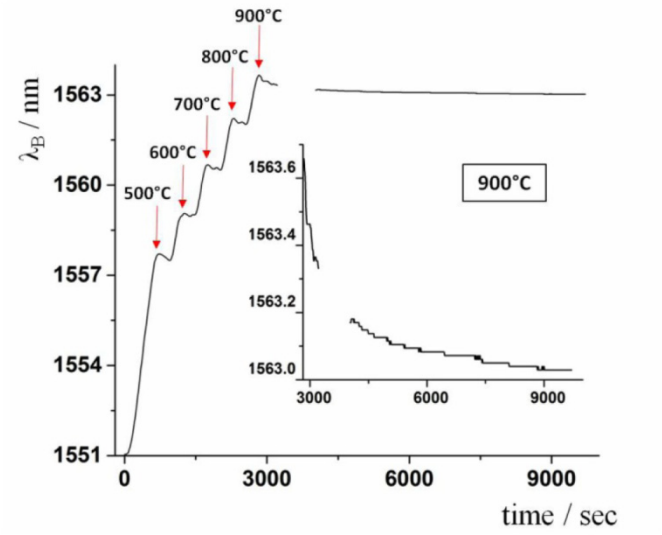

Fig. 2. λ_B change during step by step annealing cycle and during isothermal holding at 900 °C (figure inset)

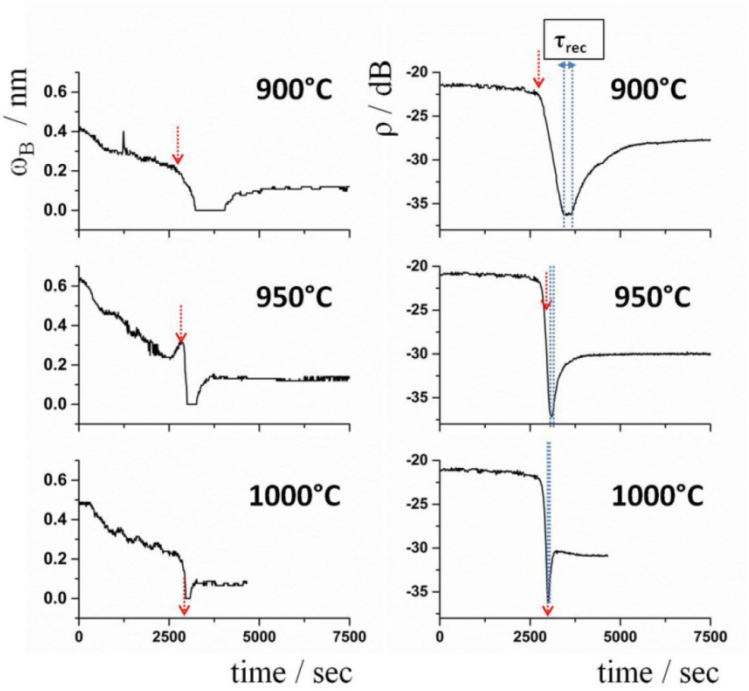

Fig. 3. The variation of $\Delta\omega_B$ and ρ during thermal regeneration process.

The thermo-optic effect *n(T)* dominates over thermal expansion so that typically 90% of the observed wavelength shifts are attributed to changes of the refractive index of the fiber core [20]. While holding the sample at T_{final}, the peak reflectivity drops to the noise level thus becoming undetectable, and after the recovery time τ_{rec} it recovers slowly and nonlinearly to a value smaller than the initial one. Simultaneously, the peak width drops to zero, then becomes undetectable during the absence of a detectable reflectivity and recovers to a value

Optics EXPRESS

which is also inferior to the initial peak width [Fig. 3]. As far as the peak reflectivity is concerned, the process is referred to as FBG regeneration. During isothermal treatment, the Bragg wavelength decreases slowly [Fig. 2] while the noise level remains unaltered.

In Figs. 4(a)-4(f), we compare the measured peak reflectivity (ρ_B) with that obtained from the amplitude of the index modulation determined from independent measurements of ω_B and λ_B, using Eqs. (2) and (3) which required the use of a parameter related to N, n_{eff} and η. Considering this parameter constant over time, shows a good overlap of the measured and calculated data in Fig. 4. These data are obtained for regeneration experiments conducted at 700 to 1000 °C. The good agreement between these curves makes our simultaneous independent measurements consistent with theoretical predictions. It indicates that all peak reflectivity variations during the regeneration process can be almost entirely attributed to the variation of the refractive index modulation inside the fiber core. This suggests that both the fraction of light inside the fiber core and the number of Bragg gratings remain unchanged during and after thermal regeneration. While the latter is not a surprise, the fact that the fraction of light inside the fiber core remains constant allows us to consider this as a one-dimensional problem along the fiber axis, with negligible contributions from radial modifications. This corresponds to the fact that the fiber core diameter is one order of magnitude larger than the grating wavelength.

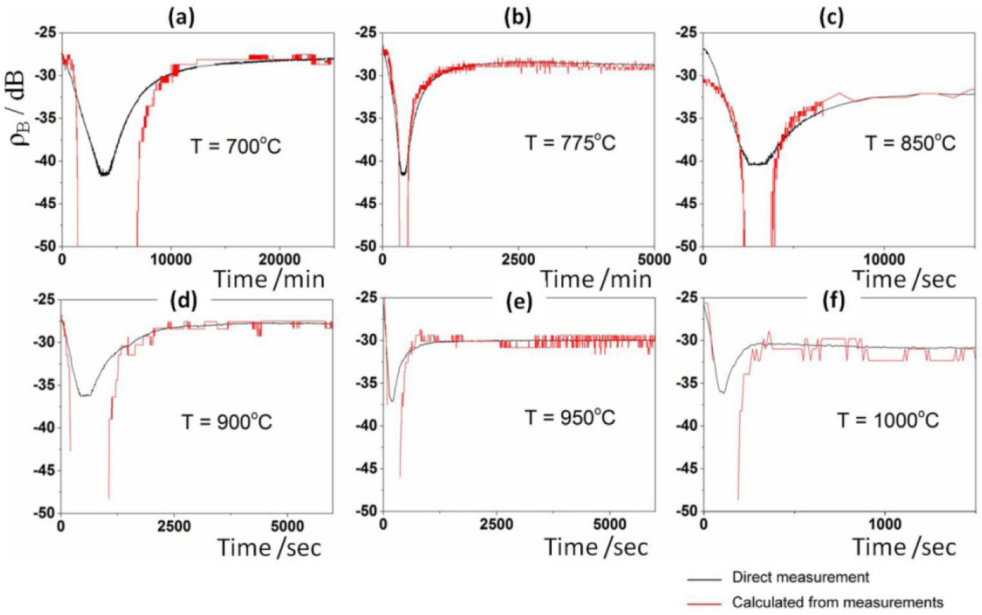

Fig. 4. (a-f) show the comparison between the measured Bragg peaks intensity (ρ_B) with that obtained from the amplitude of the index modulation determined from independent measurements of ω_B and λ_B.

4. Effect of regeneration temperature

4.1. Process efficiency and long-term stability

In the present work, instead of using a two-step annealing process as described in previous studies [6, 21], thermal regeneration was conducted isothermally (upon reaching T_{final}) in the 700-1000 °C temperature range. As we observed that regeneration was possible at all investigated temperatures, we obtained a clear understanding of the effects related to the isothermal temperature (T_{final}) on the regeneration efficiency. In Fig. 5(a), we plot the recovery rate determined from OSA measurements upon regeneration as a function of T_{final}.

Optics EXPRESS

From 700 to 1000 °C, we found an inverse relationship between T_{final} and the percentage of the peak reflectivity recovered after thermal regeneration. The latter reaches a remarkable maximum of 85.2% at 700 °C, and a minimum of 10.1% at 1000 °C. The time evolution of the peak reflectivity measured at 700 °C is presented in Fig. 5(b). However, as expected, the time necessary for a complete regeneration process increases substantially at low temperatures: it required 450 hours at 700 °C compared to 1.3 hours at 1000 °C.

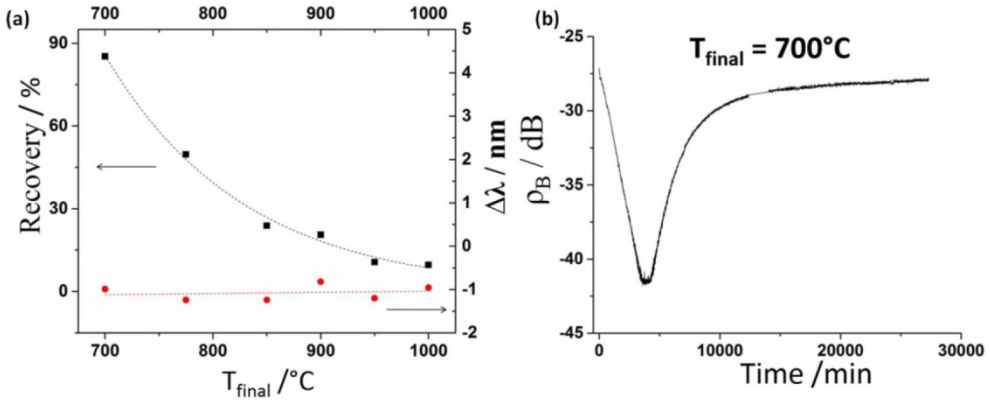

Fig. 5. (a) shows the plots of regeneration recovery (%) vs. T_{final}, and $\Delta\lambda$ vs. T_{final} (b) thermal regeneration at T_{final} = 700 °C (ρ vs. time).

In addition, a higher peak reflectivity generates longer operation times of RFBG-based thermal sensors at high temperatures, because a more intense reflectivity will have better wavelength precision for temperature sensitivity for longer durations. Also, at very high temperatures the decay time of the higher peak reflectivity will be longer. To determine the differences in long-term thermal stabilities of RFBGs developed at (T_{final}) 700 °C (I) and 775 °C (II), we conducted isothermal treatments at 1000 °C. RFBG-I is initially regenerated at 700 °C with 85.2% reflectivity, and then after the furnace is cooled to RT, long-term annealing at 1000 °C for 500 hours was conducted. Similarly, RFBG-II was regenerated at 775 °C with a reflectivity of 49.7%, and then annealed at 1000 °C for 140 hours. The variation in ρ_B upon long-term thermal exposure given in Fig. 6(a) indicates the superior thermal stability at 1000 °C of the grating regenerated at 700 °C (I) compared to the one regenerated at 775 °C (II). The higher peak reflectivity of RFBG (I) upon isothermal treatment at 1000 °C even after 500 hours is shown in Figs. 6(b) and 6(c) in comparison to the RFBG-II reflectivity after only 140 hours at 1000°C. Such increase in the thermal stability via regeneration at a lower T_{final} represents a significant added-value for FBG-based thermal sensors used in harsh environments because it significantly extends their operability. The final reflectivities of RFBG-I and RFBG-II were determined to be 43.8% and 15.9%, respectively. Hence, upon long-term thermal exposure (1000 °C, 500 hrs) RFBG-I preserves a high peak reflectivity with low degradation (Figs. 6(b) and 6(c)).

For thermal sensor reliability assessment, calibration measurements were conducted in the 26-1000 °C temperature range for RFBG-I with four repetitions [Fig. 6(d)]. Calibration curves, which are crucial for FBG sensors intended for industrial applications, indicate high repeatability. Wavelength measurements at 11 different temperatures for each calibration cycle are the average values of around 100 measurements. The maximum wavelength shift for a certain temperature was determined to be around 30 pm which corresponds to 2 °C. Hence, temperature values as a function of wavelength can be determined with maximum ± 2°C error [Fig. 6(d)].

Optics EXPRESS

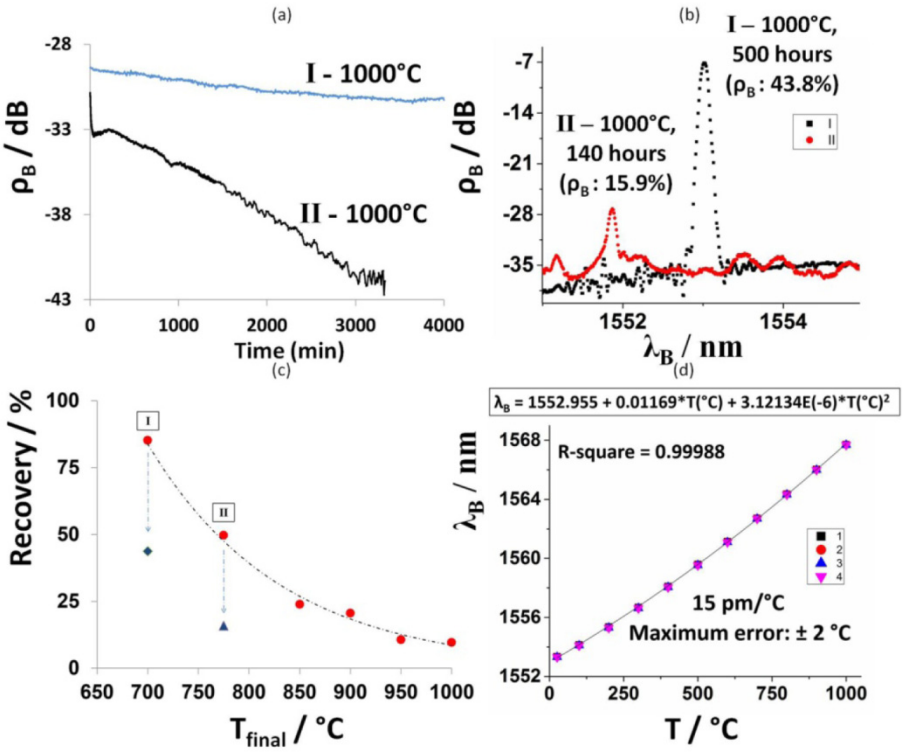

Fig. 6. (a) Superior long-term stability of (b) RFBG-I compared to RFBG-II at 1000 °C. (c) Decrease in recovery (%) as shown with arrows upon long-term heat exposure at 1000 °C. (d) Calibration curves of RFBG-I sensor (26 °C to 1000 °C)

4.2. Bragg wavelength shifts

The total change in wavelength was determined from λ_B values (in nm) at RT before (λ_i) and after regeneration (λ_f). Figure 5(a) shows the overall change in wavelength ($\Delta\lambda = \lambda_f - \lambda_i$) variation at different T_{final}. A constant blueshift of ~1 nm (± 0.2 nm), independent of the isothermal temperature, occurs upon regeneration. The difference in λ_B before and after the heating cycle depends on the depth of the FBG as expressed in decibel (dB) of peak reflectivity. A continuous blueshift (as presented in Fig. 2) was also observed in thermal decay studies conducted isothermally at very low temperatures (T < 400 °C) without the involvement of the regeneration process [22, 23]. The decrease in wavelength at constant temperature, which is attributed to the decay of the average refractive index of the fiber core, obeys a power-law [22, 23]. Discrepancies between experimental data and model were observed at higher temperatures (T > 400 °C) where a redshift occurred and was attributed to the presence of Boron in the cladding [22, 23]. Nevertheless, since the spectral shifts cannot be neglected during the ramp [Fig. 2], extracting accurate quantitative information from an analysis of this wavelength decay can lead to erroneous conclusions.

On the other hand, in a regeneration study conducted on fibers with 14-15% B_2O_3 and 10 mol% GeO_2, a continuous blueshift during isothermal treatment as well as a total $\Delta\lambda$ of ~2.1 nm (blueshift) were observed. This wavelength shift was attributed to the relaxation of core/cladding stress resulting in the reduction of the effective optical index [19]. On the contrary, *Lai et al.* related the blueshift of the wavelength to the inhibition of the structural relaxation in the core of the fiber via an increase in the T_g of glass fibers [24].

In the present study, the most important result obtained for measured spectral shifts is related to their temperature-independence, indicating that the difference between initial and

Optics EXPRESS

stabilized Bragg wavelengths is not correlated with the regeneration efficiency. We associate this feature with a global increase of the tensile stress between the fiber core and the cladding, resulting from a structural densification of the whole fiber core during thermal regeneration. Such a variation of the fiber core volume induces changes of both the effective refractive index (Δn_{eff}) and the stress condition ($\Delta\sigma_z$), which can be expressed as follows [25]:

$$\Delta n_{eff} = n_{eff}\left(\frac{\lambda i}{\lambda f} - 1\right) \tag{4}$$

$$\sigma_z = \frac{2\Delta n_{eff}}{3C_2 + C_1} \tag{5}$$

where λ_i and λ_f are the initial and final Bragg wavelengths, respectively, and C_1 and C_2 are the axial stress confining coefficients. From an effective refractive index reduction of about 0.07% obtained in this study, the change of axial stress can be estimated to be around 30.0 kg/mm^2 from stress optic coefficients $C_1 = 4.102 \times 10^{-5}$ mm^2/kg and $C_2 = 7.42 \times 10^{-6}$ mm^2/kg [25]. A similar axial stress value was reported for a fiber with 125 μm in diameter [25].

4.3. Activation energy

We report the temperature dependence of '*recovery time*', τ_{rec}, defined as the duration between the disappearance of the reflectivity in the background noise (t_a) and the appearance of the reflectivity (t_b), to determine the activation energy of recovery (E_{rec}). This approach is used to replace more complex curve-fitting functions using decay time dependence to varying temperatures with a simple time-temperature relationship [13, 26–28]. We assume that the time at which the reflectivity disappears in the background noise after t_a, is a reference point similar to all experiments conducted at different T_{final}. Hence, even though the regeneration process has not yet started at t_a, $\tau_{rec} = (t_b - t_a)$ can be considered as the incubation period for the onset of the regeneration process. As shown in Fig. 3, τ_{rec} depends on the temperature and its dependence is further investigated. As an FBG consists of periodic refractive index modulations in the fiber core, the thermal process responsible for the so-called 'regeneration' should be active between these periods at a fixed distance. Therefore, the basic characteristic diffusion length [Eq. (6)] can be used during τ_{rec}.

$$\chi = \sqrt{Dt} \tag{6}$$

$$A - \ln t = -\frac{E}{k_B T} \tag{7}$$

where $D = D_0 e^{\left(-\frac{E}{k_B T}\right)}$, χ is the fixed length and A is constant ($A = \ln \chi^2 - \ln D_0$)

Equation (7) is derived using Eq. (6) and accordingly ln τ_{rec} vs. 1000/T plot was drawn covering the all temperature range (700-1000°C). A linear relationship was found, as shown in Fig. 7. The activation energy of recovery, E_{rec}, from the slope of the linear curve (Ln τ_{rec} vs. 1000/T) was determined as 2.64 (± 0.13) eV. The most significant error in measuring τ_{rec} from the reflectivity is due to the scattering in the initial background noise level that depends on various factors, including the quality of splicing, the deviation of the cut fiber surface in the open end and the structural variation in the fiber itself. The maximum scattering in the background is found to be ~0.7 dB. Hence, the error bars indicated in Fig. 7 are calculated from the variation of background levels and subsequent recovery time, labelled as τ_{rec}'.

Optics EXPRESS

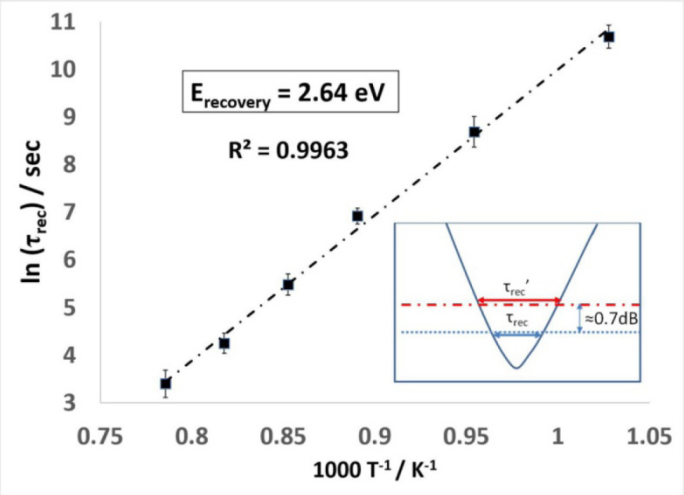

Fig. 7. Plot of ln (τ_{rec}) vs. 1000/T covering the all temperature range (700-1000°C).

Although activation energy values should depend on both fiber composition and FBG specifications, similar values have already been reported by different research groups using mainly the curve fitting approach [26–28]. We found that such an activation energy was consistent with the model proposed by *Erdogan et al.* [26], who associated the grating decay phenomenon with a de-trapping mechanism of electrons based on a distribution of activation energies peaked at around 2.80 eV (± 0.19 eV) for an Er-doped FBG. Another study based on a similar approach showed two different activation energy distributions for type-I (2.14 eV) and type-IIA (2.45 eV) gratings written on Boron (B)-Germanium (Ge) co-doped silica fibers [27]. Other thermal decay studies also reported activation energies ranging from 2.2 to 3.1 eV on FBGs with different fiber compositions [29, 30]. More recently, *Holmberg et al.* [13] determined two activation energy values of 3.05 eV and 0.89 eV via the rate of change in refractive index modulation and Bragg wavelength changes, respectively. It was stated that these energy values are due to diffusion-reaction dynamics of molecular water in silica glass [13]. On the other hand, a diffusional study conducted by *Zhou et al.* [31] reported an activation energy of 2.63 eV (similar to E_{rec} 2.64 eV determined in this present study) for the removal of hydroxyl from silica glass in a temperature range of 700-900 °C.

To obtain complementary information regarding possible structural changes during regeneration, we performed PL measurements and optical imaging on FBG before and after regeneration at 775 °C. The measurements were carried out at RT, using an experimental approach that allowed us to connect the periodic refractive index modulation of the fibre core with local variations of oxygen-related defect emission [32]. Figure 8 displays the PL spectra recorded for a laser excitation spot focused inside the fiber core indicating a broad PL emission around ~560 nm (2.2 eV) which originates from multiple sources of oxygen defects in silica matrix. Oxygen defects (Non-Bridging Oxygen Hole Centers (NBOHC) ~517-620 nm (2-2.4 eV), Peroxy radicals ~629 nm (1.97 eV) and Si Oxygen Deficiency Centers (ODC) ~440-460 nm (2.7-2.8 eV)) [33–35] generated during the FBG writing disappear during the regeneration process. Moreover, FBG modulation seen in optical images [Fig. 8] before regeneration was not observable after thermal regeneration at 775 °C. The removal of oxygen defects through diffusional transport is consistent with the densification of the whole fiber core (evoked in sec. 4.2), which reduces the concentration of chemical dangling bonds. It can also be related to the disappearance of initial FBG refractive index modulation during thermal regeneration process, thus suggesting that the modulation before and after

Optics EXPRESS

regeneration may have different origins. This is in agreement with the fact that the thermal stability of peak reflectivity increases significantly upon the completion of regeneration.

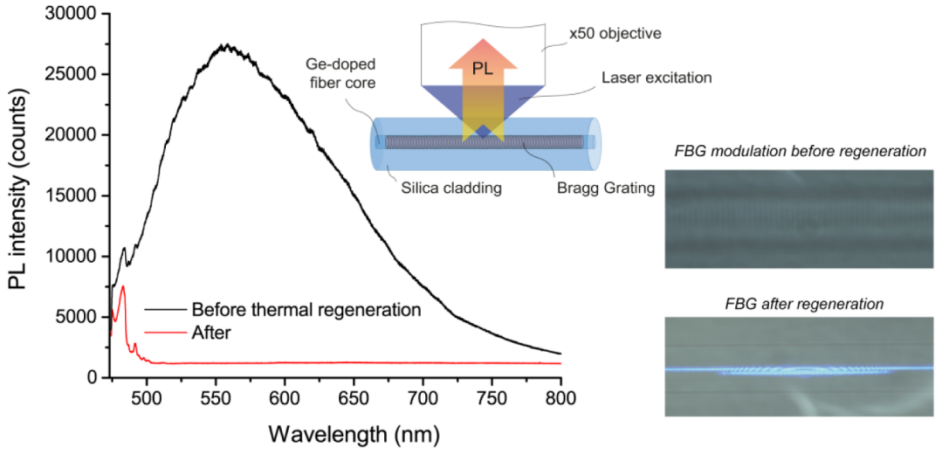

Fig. 8. PL spectra and optical images obtained before and after thermal regeneration process at 775 °C.

5. Comments on the regeneration mechanisms

Several studies associated the thermal regeneration with mechanisms of different origins, involving complex atomic diffusion or stress induced densification of the fiber core [4, 12, 13, 19]. Thermal diffusion related phenomena were suggested by Fokine *et al.* [36, 37] who developed CCG systems with refractive index modulations resulting from spatially periodic variations of fluorine (F) and oxygen (O) dopant concentrations. However, since the activation of these diffusion mechanisms was stated to be dependent on the presence of hydroxyl (OH) groups, such a scenario should not permit to regenerate B/Ge doped silica fibers after Helium loading [18], a remarkable feature demonstrated by Canning *et al.* [15] who correlated the main mechanism responsible for thermal regeneration with the occurrence of stress induced densification effects. In this latter approach, it is suggested that UV inscription induces a periodic pressure modulation inside the fiber core, which promotes the formation of a cristobalite phase during thermal annealing. Higher thermal stability of cristobalite compared to amorphous silica causes stronger gratings that can extend the temperature range of FBG operation up to 1295 °C [15].

This study presents regeneration experiments performed within a temperature range of 700-1000 °C, showing that lower temperatures (T_{final}) improve the regeneration efficiency as well as the long-term stability of RFBG sensors [Fig. 6]. As described earlier in section 4.3, the thermal regeneration process dynamics during 'recovery time' was found to follow an Arrhenius type behaviour as verified by the linear dependence of ln τ_{rec} vs. 1000/T, giving an activation energy of 2.64 (± 0.13) eV. The derivation of the characteristic diffusion length [Eq. (6)] was used on the assumption that if diffusional processes play a role in the thermal regeneration process as reported in previous studies [36, 37], diffusion should take place between equally spaced grating periods of about 500 nm. The linearity between ln τ_{rec} and 1000/T shown in Fig. 7 is an indication that the assumption is feasible and diffusional processes involve in the thermal regeneration process. A single activation energy, consistent with the reported activation energy values obtained in previous studies by thermal decay and regeneration investigations conducted on FBGs with varying compositions and thermal treatment, shows that one type of diffusional transport is dominantly active during thermal regeneration between 700 and 1000 °C. In addition, the disappearance of oxygen-related defects upon thermal regeneration indicates that diffusion takes place in this process.

Optics EXPRESS

Nevertheless, a regeneration theory based only on diffusion related mechanisms does not adequately describe the increase in recovery rate at lower regeneration temperatures, because higher thermal activation should promote atomic motion.

On the other hand, models referring to stress induced densification as the main mechanism for thermal regeneration are not consistent with our experimental findings regarding the overall wavelength shifts. The fact that these wavelength shifts do not depend on the regeneration temperature indicates that stress relaxations are not quantitatively correlated with final peak reflectivities upon regeneration. Therefore, we attributed this overall blueshift to a release of tensile stress between core and cladding. Its continuous evolution during thermal regeneration suggests a continuous increase in the T_g of the fiber core, which is compatible with glass densification. This assumption is partially consistent with scenarios in which the main mechanism responsible for the thermal regeneration process is the crystallization of amorphous silica into the cristobalite phase [15], but our results evidence here that such mechanisms cannot be the primary cause of the increase in recovery rates. Even if we cannot exclude that the densification of the core can strongly affect the periodic mechanical constraints at the core/cladding interface, resulting from the Bragg grating inscription, such a scenario is insufficient to describe the evolution of the peak reflectivity over the whole duration of the regeneration process.

As a consequence of these experimental findings, we infer that both diffusional phenomena and stress induced mechanisms take part in the thermal regeneration process. For the moment, none of the proposed theories can describe the dependence of recovery efficiency of peak reflectivity on the regeneration temperature. This necessitates further investigations based on a new theoretical approach, which takes into account several contributions of different origins to the periodic refractive index modulation.

6. Conclusions and perspectives

In this work we examined the role of annealing temperature on the thermal regeneration process. We determined an inverse relationship between the temperature of regeneration and recovery efficiency reaching 85.2% at 700 °C. The long-term stability of regenerated reflectivity over 500 hours at 1000 °C exhibits great potential to be used as thermal sensors for space applications. Calibration measurements showed the high repeatability and reliability of RFBG sensors up to 1000 °C. Process dynamics was found to follow an Arrhenius type behaviour during recovery time where no reflectivity is detectable. The experimental data suggest the involvement of both diffusion dependent processes as well as stress evolution due to the densification of the fiber core. Hence, the role of both mechanisms should be considered for a clear understanding of the thermal regeneration process. Based on these results, new theoretical models capable of explaining both the diffusion and stress related mechanisms should be developed. Further investigations aiming to optimize parameters such as seed-grating strength and fiber photosensitivity on regeneration dynamics may shed light into the origins of the thermal regeneration process. These studies will allow us to understand the limits of this process for developing optimal performance FBG sensors.

Funding

This work was supported by the NSERC Strategic Grant STPGP 447377-13 in partnership with MPB Technologies.

Acknowledgments

The authors would like to thank Dr. Émile Haddad and Kamel Tagziria from MPB Technologies Inc., and Mr. Iain McKenzie from the European Space Agency (ESA-ESTEC) for useful discussions. F.R. acknowledges NSERC for an EWR Steacie Memorial Fellowship. F.R. and A.R. are supported by individual Discovery Grants (NSERC).